

RESEARCH ARTICLE

10.1002/2014JF003286

Particle friction angles in steep mountain channels

Jeff P. Prancevic¹ and Michael P. Lamb¹¹Division of Geological and Planetary Sciences, California Institute of Technology, Pasadena, California, USA

Key Points:

- Friction angles in natural beds are higher due to interlocking and burial
- Mean friction angle does not change with slope or channel width at tested sites
- Relative stability of steps and large grains promotes momentum loss to form drag

Supporting Information:

- Text S1
- Data set S1
- Data set S2a
- Data set S2b
- Data set S2c
- Data set S2d
- Data set S2e
- Data set S2f
- Data set S2g
- Data set S2h

Correspondence to:

J. P. Prancevic,
jprancev@caltech.edu

Citation:

Prancevic, J. P., and M. P. Lamb (2015), Particle friction angles in steep mountain channels, *J. Geophys. Res. Earth Surf.*, 120, doi:10.1002/2014JF003286.

Received 17 JUL 2014

Accepted 14 JAN 2015

Accepted article online 16 JAN 2015

Abstract Sediment transport rates in steep mountain channels are typically an order of magnitude lower than predicted by models developed for lowland rivers. One hypothesis for this observation is that particles are more stable in mountain channels due to particle-particle interlocking or bridging across the channel width. This hypothesis has yet to be tested, however, because we lack direct measurements of particle friction angles in steep mountain channels. Here we address this data gap by directly measuring the minimum force required to dislodge sediment (pebbles to boulders) and the sediment weight in mountain channels using a handheld force gauge. At eight sites in California, with reach-averaged bed angles ranging from 0.5° to 23° and channel widths ranging from 2 m to 16 m, we show that friction angles in natural streams average 68° and are 16° larger than those typically measured in laboratory experiments, which is likely due to particle interlocking and burial. Results also show that larger grains are disproportionately more stable than predicted by existing models and that grains organized into steps are twice as stable as grains outside of steps. However, the mean particle friction angle does not vary systematically with bed slope. These results do not support systematic increases in friction angle in steeper and narrower channels to explain the observed low sediment transport rates in mountain channels. Instead, the spatial pattern and grain-size dependence of particle friction angles may indirectly lower transport rates in steep, narrow channels by stabilizing large clasts and channel-spanning steps, which act as momentum sinks due to form drag.

1. Introduction

Sediment within mountain channels moves intermittently. During active transport, sediment attacks the underlying bedrock, driving incision [e.g., *Sklar and Dietrich*, 2004]. In large flood events, high sediment transport rates, and debris flows may pose serious hazards to life and infrastructure [e.g., *Rickenmann*, 2012; *Prancevic et al.*, 2014]. Between transport events, sediment provides structure to the channel bed [e.g., *Church et al.*, 1998] that creates habitat for riverine fauna [e.g., *Coulombe-Pontbriand and Lapointe*, 2004] and partly determines water flow rates [e.g., *Aberle and Smart*, 2003]. Thus, determining the stability of sediment is necessary to better understand the evolution of mountainous landscapes and riverine habitats. Despite its importance, there are very few direct measurements in steep mountain streams of the particle friction angle, one of the key metrics of bed stability.

Sediment transport is the result of the driving fluid stress (skin friction and form drag) overcoming the resistive stress derived from the gravitational stability of a grain in its pocket between other grains (Figure 1a) [e.g., *Gilbert*, 1914; *Shields*, 1936; *Wiberg and Smith*, 1987]. Both sides of this stress balance exhibit complicated behavior due to turbulent fluid flow [e.g., *Schmeeckle et al.*, 2007], complex bed geometry [e.g., *Zimmermann and Church*, 2001], and a mixture of grain shapes and sizes [e.g., *Miller and Byrne*, 1966]. Consequently, the full distribution of driving stress-resisting stress combinations is difficult to predict, and we typically rely on representative, empirical relationships for predicting initial motion and bed load transport rates. These relationships were initially developed for application to lowland rivers [*Shields*, 1936; *Meyer-Peter and Mueller*, 1948; *Miller and Byrne*, 1966] and are inadequate in describing sediment transport in steep, coarse-bedded environments, where bed load transport rates are typically an order of magnitude smaller than predicted [e.g., *Rickenmann*, 1997; *Yager et al.*, 2007; *Mueller et al.*, 2008]. Even the onset of sediment transport in steep channels requires significantly higher bed shear stresses than expected [*Bartnick*, 1991; *Mueller et al.*, 2005; *Lenzi et al.*, 2006b; *Scheingross et al.*, 2013]. There is debate as to whether the divergence between predictions and observations in steep channels is due to changes in granular stability, changes in flow hydraulics, or both [e.g., *Church et al.*, 1998; *Yager et al.*, 2007; *Lamb et al.*, 2008; *Recking*, 2009; *Zimmermann et al.*, 2010; *Ferguson*, 2012]. Flume experiments with loose, unimodal sediment beds show that sediment stability increases and bed load transport rates are reduced in steeper channels with respect to predicted values, suggesting that

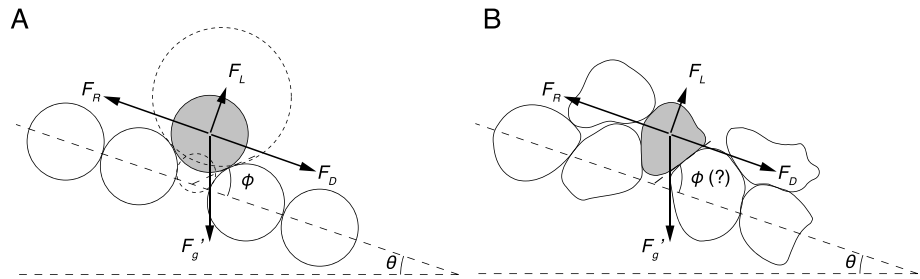


Figure 1. Two-dimensional schematics of (a) an idealized grain-pocket configuration and (b) a more realistic pocket with wedged and imbricated grains with relevant force vectors shown. The dotted circles in Figure 1a illustrate the theorized effect of changing D/D_{50} on the particle friction angle. The small circle has a size of $D/D_{50} = 0.5$, and the large has a size of $D/D_{50} = 1.8$.

these effects are in part due to changes in hydraulics [e.g., Gregoretti, 2008; Prancevic et al., 2014]. Changes in grain stability have been difficult to evaluate in natural steep channels, however, due to limitations of standard measurement techniques [e.g., Miller and Byrne, 1966; Kirchner et al., 1990; Buffington et al., 1992].

The resisting force that stabilizes a particle in a sediment bed is typically formulated as a simple Coulomb friction model:

$$F_R \leq \sum_i F_{n,i} \tan \phi, \tag{1}$$

where F_R is the frictional force resisting motion, $F_{n,i}$ is the normal force exerted on grain from contact point i , and the friction coefficient is parameterized as the tangent of a friction angle, ϕ . The particle friction angle is often idealized as the angle of inclination, relative to the channel bed slope, about the contact point between the grain in question and one of its downstream neighbors (e.g., Figure 1a). This is appropriate in a simplified configuration in which, at the onset of motion, the only contact point for the grain in question is that of its downstream neighbor. In natural streambeds, this simplified configuration may not hold, however, and irregular bed packing, grain shape, and partial burial can cause multiple contact points to be important (e.g., Figure 1b).

In many studies, the friction angle is measured directly using a tilting surface composed of fixed grains (e.g., natural pebbles, sand, or spheres) [Miller and Byrne, 1966; Li and Komar, 1986; Kirchner et al., 1990; Buffington et al., 1992]. One or more grains are placed on the fixed granular surface, which is tilted until a loose grain becomes unstable, and rolls or slides out of its pocket. The angle at which this occurs is the particle friction angle, and the driving and resisting forces are equal to the weight of the grain (W) times the sine and cosine of the particle friction angle, respectively [e.g., Miller and Byrne, 1966]. It is equivalent to measure particle friction angles in situ by measuring the force required to mobilize grains in a channel bed relative to their respective weights [Johnston et al., 1998]. Laronne [1973] was the first to apply this methodology in a natural channel and the two friction angles he measured pulling parallel to the bed, $\phi = 62^\circ$ and $\phi = 76^\circ$, were much higher than those measured on tilting tables and typically assumed in bed load transport formulae. Following a similar methodology, Johnston et al. [1998] amassed the first extensive data set of in situ particle friction angles, but their study was limited to relatively low-sloping channels ($\theta < 3^\circ$) and grains that lacked sorting and imbrication [Johnston et al., 1998]. Downes et al. [1997] and Sanguinito and Johnson [2011] have also made dislodgement force measurements in natural channels.

Results from previous laboratory (tilt table) experiments and field measurements have revealed a strong dependence on the size of the diameter of the test grain (D) relative to the roughness of the granular bed (e.g., D/D_{50} , in which D_r is the n th percentile grain size). Results show that large grains are less stable than smaller ones due to their propensity to rest higher on the surrounding grains (Figure 1) and therefore at a lower angle to the average bed [Miller and Byrne, 1966; Li and Komar, 1986; Kirchner et al., 1990; Buffington et al., 1992; Johnston et al., 1998]. To capture this effect, mean friction angles for a specific grain size ($\bar{\phi}$) are typically modeled as a power law relationship:

$$\frac{\bar{\phi}}{\phi_{D_{50}}} = \left(\frac{D}{D_{50}} \right)^{-\beta}, \tag{2}$$

Table 1. Compiled Relative Grain Size Dependence

Study Location/Sediment Type	$\overline{\phi}_{D_{50}}$ (deg)	β
<i>Miller and Byrne</i> [1966]		
Natural sand	57.3	0.30
Glass spheres, poorly sorted	45.7	0.32
Glass spheres, well sorted	44.9	0.44
<i>Li and Komar</i> [1986]		
Crushed basalt	51.3	0.33
Spheres	20.4	0.75
Ellipsoidal natural grains	31.9	0.36
<i>Kirchner et al.</i> [1990] ^a		
Natural grains, poorly sorted, water worked	55.2	0.31
Natural grains, poorly sorted, unworked	66.1	0.46
<i>Buffington et al.</i> [1992] ^a		
Natural sediment surface, $K_s = 4.1$ mm	60	0.26
Natural sediment surface, $K_s = 11.4$ mm	51	0.28
Natural sediment surface, $K_s = 14.0$ mm	54	0.21
Natural sediment surface, $K_s = 14.5$ mm	46	0.21
Natural sediment surface, $K_s = 45.0$ mm	52	0.24
<i>Johnston et al.</i> [1998] ^a		
Pacific Creek	61.9	0.28
Van Duzen River	49.1	0.45
Sagehen Creek	51.6	0.30
Colorado River	55.5	0.14
Present study		
Sespe Creek Thalweg	66.4	-0.01
Sespe Creek Bar	73.5	-0.01
Rose Valley Tributary	67.5	-0.01
Arroyo Seco	69.2	-0.01
Block Creek	69.9	0.18
San Oline Creek	67.7	0.18
Tumble Creek	64.3	0.18
Rattlesnake Creek	67.3	0.18

^a $\overline{\phi}_{D_{50}}$ refers to the median friction angle of the median grain size in *Kirchner et al.* [1990], *Buffington et al.* [1992], and *Johnston et al.*'s [1998] studies. In all other studies, $\overline{\phi}_{D_{50}}$ refers to the mean friction angle of the median grain size.

where $\overline{\phi}_{D_{50}}$ is the mean friction angle of the median grain size and β is an empirical constant, with typical ranges of $\overline{\phi}_{D_{50}} = 46^\circ$ to 66° and $\beta = 0.21$ to 0.46 for natural grains (Table 1). This relative grain size dependence in particle friction angle promotes mobility of larger grains relative to smaller grains, partially offsetting differences in grain weight [e.g., *Wiberg and Smith*, 1987; *Solari and Parker*, 2000]. However, no friction angle data exist for steep mountain streams ($\theta > 3^\circ$), where particle mobility has been observed to be highly size selective [e.g., *Brummer and Montgomery*, 2003; *Scheingross et al.*, 2013].

While there have been no direct measurements of particle friction angles in steep natural channels ($\theta > 3^\circ$), observations of sediment transport provide clues that grain stability may increase there relative to low-sloping channels. Researchers typically report sediment transport rates as a function of total bed shear stress (τ_b) normalized by grain diameter (D), termed Shields stress: $\tau^* = \frac{\tau_b}{(\rho_s - \rho)gD}$, where g is the acceleration due to gravity, ρ is the material density of water, and ρ_s is the material density of sediment. Measurements at the onset of sediment motion

reveal that grains require increased Shields stress to move in steeper channels in both the field [*Bartrick*, 1991; *Andrews*, 1994, 2000; *Church and Hassan*, 2002; *Mueller et al.*, 2005; *Lenzi et al.*, 2006a; *Whitaker and Potts*, 2007; *Mao et al.*, 2008; *Scheingross et al.*, 2013] and laboratory flumes [*Ashida and Bayazit*, 1973; *Bathurst et al.*, 1984; *Olivero*, 1984; *Graf and Suszka*, 1987; *Torri and Poesen*, 1988; *Picon*, 1991; *Shvidchenko and Pender*, 2000; *Gregoretto*, 2008; *Prancevic et al.*, 2014] (Figure 2). In addition, the threshold Shields stress required to mobilize material in the field is higher relative to flume experiments for a given bed slope (Figure 2). Researchers have also identified a correlation between changes in channel width and the threshold Shields stress such that narrower channels have grains that appear more stable [*Zimmermann et al.*, 2010] (Figure 3). Finally, this increased stability appears to continue after initial transport, and sediment transport rates are typically an order of magnitude smaller than predicted by sediment transport equations developed for lowland rivers [*Rickenmann*, 1997; *D'Agostino and Lenzi*, 1999]. Despite observations that point to enhanced grain stability in steep streams, it remains an open question as to what degree this stability is due to enhanced granular friction or reduced effectiveness of water flow in transporting sediment with increasing channel slope.

One mechanism to increase particle friction angles that is inherent to increased bed angle is the potential for increased normal forces from neighboring grains. In imbricated packing arrangements, grains become increasingly vertically stacked as slope increases. This, however, should only have a strong effect on very steep slopes ($\theta \gg 6^\circ$), where the downstream component of gravity is of the same order as the bed-normal component. More complex grain interactions, including interlocking and jamming, may provide an additional means to alter particle friction angles. Grains in steep channels also tend to be more angular due to their small

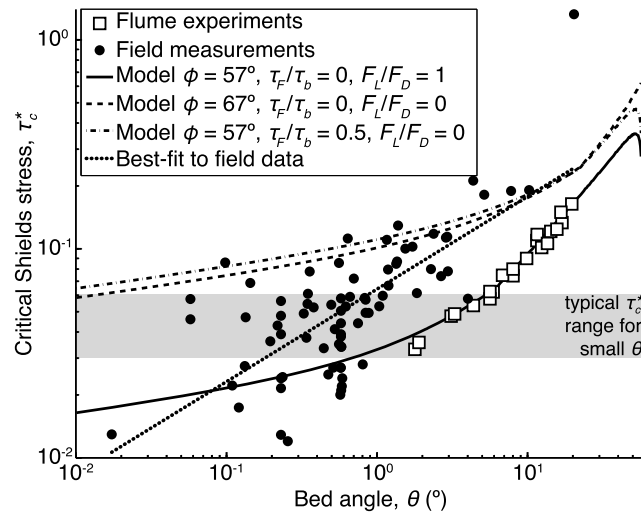


Figure 2. Compilation of field data and a subset of flume data [Prancevic et al., 2014] showing critical Shields stress at the onset of motion as a function of bed slope. The theoretical force balance of Lamb et al. [2008] is shown in the solid, dashed, and dash-dotted lines for various scenarios. The dotted line is the best fit curve to the compilation of field data (includes data from Buffington et al. [1997] review and Andrews [1994, 2000], Church and Hassan [2002], Whitaker and Potts [2007], Mao et al. [2008], and Scheingross et al. [2013]), which are used for subsequent predictions of particle friction angle changes as a function of slope. Note that the exponent of this power law, $\tau_c^* = 0.39 \tan \theta^{0.44}$, is larger than the fit presented in Lamb et al. [2008], $\tau_c^* = 0.15 \tan \theta^{0.25}$, which includes both field and flume data and lacks data from Scheingross et al. [2013].

transport distances. Angular grains are known to have high particle friction angles from tilt table experiments [Miller and Byrne, 1966], but the role of angularity in stabilizing grains may be more substantial in natural channels due to increased grain interaction.

Additional processes that may affect bed stability in steep mountain channels but are not present in lower sloping rivers ($\theta < \sim 1^\circ$) are the transport and deposition of debris flow material. The random grain organization of debris flow deposits relative to fluvial deposits may cause differences in grain stability [Major, 1997]. Erosional (e.g., scour marks and plucking) and depositional (e.g., levees and snouts) evidence for debris flow transport may be found throughout the channel network steeper than $\theta > \sim 1^\circ$ due to long runoff distances [Stock and Dietrich, 2006]. However, experimental results suggest that fluvial transport can occur up to slopes of $\theta < \sim 22^\circ$ [Prancevic et al., 2014]. Channel beds between these two bed slopes may contain debris flow deposits that have been reworked to varying degrees by subsequent fluvial transport.

The goal of this work is to characterize the distribution of particle friction angles present on steep channel beds without bias in our selection based on patchiness or imbrication. This is in contrast to the study of Johnston et al. [1998], which explicitly avoided any portions of the bed that exhibited spatial sorting or imbrication. We use in situ measurements from a force gauge collected on bed angles ranging from $\theta = 0.5^\circ$ to 23° to test the hypothesis that increased particle friction angles in steeper channels contribute to increased threshold Shields stress. We also test the hypothesis that increased particle friction angle in natural channels compared to laboratory flumes contributes to the offset in respective threshold Shields stresses.

2. Theoretical Expectations

In order to establish baseline predictions for particle friction angle variability, we utilize the force balance model of Lamb et al. [2008] to solve for the particle friction angles that yield the observed critical Shields stress in Figures 2 and 3. In addition to particle friction angle, there are other unconstrained parameters in the model that could also be used to attempt to match the model to observations, including most notably momentum loss to form drag (which will be discussed in section 5.5). Moreover, there are other factors important in natural rivers (e.g., grain burial and bed surface patchiness) that are not incorporated in the simple 1-D model at all. Our goal in performing this exercise is not to assert that the model is correct nor that the discrepancy between model and observations is purely a result of systematic variations in particle friction angles. Rather, these comparisons are useful because they allow us to recast the qualitative hypothesis that

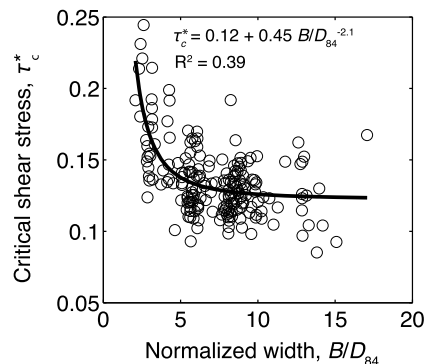


Figure 3. Adapted from experiments of Zimmermann et al. [2010] showing bed stability as a function of normalized width. The best fit curve is ours and is used in subsequent predictions of particle friction angle changes as a function of normalized width.

systematic variations in particle friction angles can explain the change in the critical Shields stress with channel slope or jamming ratio (Figures 2 and 3) into quantitative expectations that can be compared to field data. Nullifying this hypothesis, in contrast, would indicate that the trends in Figures 2 and 3 must be explained in part by other factors (e.g., enhanced form drag).

The *Lamb et al.*'s [2008] model follows that of *Wiberg and Smith* [1987] by balancing the forces pulling the grain downslope (gravity and fluid drag stress, F_D) with the frictional resisting force of the pocket, F_R . Both models calculate F_R at the onset of motion by substituting the total normal force in equation (1) with the weight of the grain normal to the bed minus the lift force:

$$F_R = [(\rho_s - \rho)V \cos \theta - F_L] \tan \phi, \quad (3)$$

where V is the volume of the particle and F_L is the hydrodynamic lift force pulling the grain away from the bed (e.g., Figure 1). By solving for the lift and drag forces in terms of bed shear stress, they present an expression for the Shields stress at the onset of motion as an explicit function of flow velocities around the grain:

$$\tau_c^* = \left(\frac{1}{1 - \tau_f/\tau_b} \right) \frac{2}{C_D \delta} \frac{u_*^2}{\langle u^2 \rangle} \frac{\tan \phi \cos \theta - \sin \theta}{1 + F_L/F_D \tan \phi} \quad (4)$$

where τ_f/τ_b is the ratio of bed shear stress expended on morphologic form drag to the total bed shear stress, C_D is the empirical drag coefficient that is set to 0.9 following *Lamb et al.* [2008], δ is a geometric variable that adjusts according to the grain's exposure to and emergence from the flow [*Lamb et al.*, 2008], $u_* = \sqrt{\frac{\tau_b}{\rho}}$ is the shear velocity of the flow, u is the time-averaged velocity, the angle brackets indicate spatial averaging over the cross-sectional area of the grain, and F_L/F_D is the ratio of lift to drag forces acting on the grain. We can also solve equation (4) explicitly for particle friction angle:

$$\tan \phi = \frac{\left(\frac{1}{1 - \tau_f/\tau_b} \right) \frac{2}{C_D \delta} \frac{u_*^2}{\langle u^2 \rangle} \sin \theta + \tau_c^*}{\left(\frac{1}{1 - \tau_f/\tau_b} \right) \frac{2}{C_D \delta} \frac{u_*^2}{\langle u^2 \rangle} \cos \theta - F_L/F_D \tau_c^*}, \quad (5)$$

allowing us to calculate the expected particle friction angle given a threshold Shields stress and some constraint on the velocity profile, drag coefficient, lift-to-drag ratio, and stress loss to form drag.

It is important to note that the lift force presented in equations (4) and (5) is assumed to reduce the frictional resistance by directly reducing the normal force in equation (1). This is appropriate if the parameterization of normal forces in equation (3) is correct. However, if there are additional normal forces from the weight and interlocking of surrounding grains (e.g., Figure 1b), the effect of lift force on the grain of interest is convoluted by the effect of lift force on the surrounding grains. In addition, direct measurements of lift forces have shown that the lift force is consistently much smaller than drag force and it does not increase with increased drag force as expected [*Schmeeckle et al.*, 2007]. Because we cannot reliably predict the effect of lift force on particle motion, we consider a range in lift-to-drag forces between $0 \leq F_L/F_D \leq 1$ for our model predictions.

In order to apply equation (4) to steep, shallow flows, the *Lamb et al.*'s [2008] model incorporates hydraulic changes observed in shallow conditions. The model applies a quadratic bed-normal velocity profile, $\frac{u}{u_*} = \frac{z}{0.12D_{50}} \left(1 - \frac{z}{2H} \right)$, where z is the distance from the mean bed elevation and $z=H$ at the water surface (following data from *Nikora et al.* [2001]). In addition, it accounts for reduced turbulent intensity in shallow flows, $\frac{\sigma_u}{u_*} = 0.2 \left[5.62 \log \left(\frac{H}{D_{50}} \right) + 4 \right]$, where σ_u is the temporal standard deviation of flow velocity at the tops of grains (following data from *Carollo et al.* [2005]). In cases where the depth of flow is smaller than the size of the bed sediment, the model includes the effects of reduced buoyancy and cross-sectional exposure by adjusting δ in equation (4) following *Lamb et al.* [2008]. Inclusion of these slope-dependent effects results in an acceptable fit to the experimental data without momentum loss to morphologic form drag [*Prancevic et al.*, 2014] (Figure 2). The friction angle used to compare the Lamb model against *Prancevic et al.*'s [2014] experimental study ($\phi = 57^\circ$) was measured using a fixed-bed tilt table, which mimicked the conditions of a fluvially unworked bed surface, devoid of interlocking and steps.

The trend of increased threshold Shields stresses on steeper slopes is offset to even higher values in the field, as compared to flume experiments (Figure 2). This offset is typically attributed to form drag. It has been well established that fluid momentum is consumed by the large pressure differential across bed forms

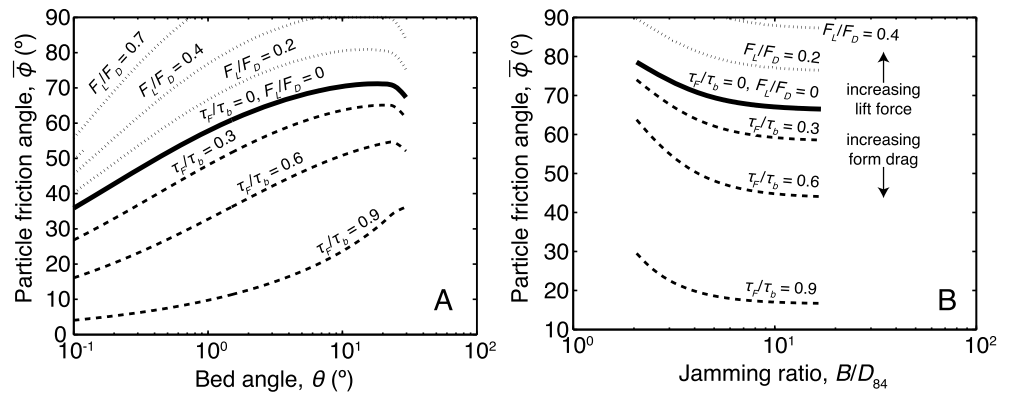


Figure 4. Predicted particle friction angle as a function of (a) bed angle and (b) jamming ratio. Predictions were calculated using a best fit to the available field data (Figure 2) and flume data (Figure 3) and equation (7). The solid line in each plot is the model prediction for no morphologic form drag and no lift force. The dashed lines are the contours with no lift force ($F_L/F_D = 0$) but increasing morphologic form drag. The dotted lines are the contours with no form drag ($\tau_f/\tau_b = 0$) but increasing lift force.

caused by flow separation [e.g., *Smith and Mclean, 1977; Kostaschuk et al., 2004*]. If the pressure differential that results from this separation acts on an immobile obstacle (e.g., large bed form or boulder) rather than mobile grains, then the total stress required to transport sediment increases. The stress lost to these obstacles is termed “morphologic form drag” and is the most common explanation for the observed offset of the threshold Shields stress in field studies [e.g., *Wiberg and Smith, 1991; Millar, 1999; Nitsche et al., 2011; Ferguson, 2012; Yager et al., 2012; Scheingross et al., 2013*]. Reported ratios of stress lost to form drag and total stress range between $\tau_f/\tau_b = 0$ and 0.9 for natural rivers [*Millar, 1999*]. Alternatively, this offset may be due to differences in bed structure leading to higher particle friction angles in the field than in the laboratory. Field measurements collected by *Laronne [1973]* suggest that naturally organized beds are more stable than laboratory beds (Table 1). This observed difference in particle friction angles ($\sim 10^\circ$) could explain the majority of sediment transport data from the field, according to theoretical modeling (Figure 2).

By calculating a least squares linear regression to the log-transformed field data (Figure 2), we can input the best fit Shields stress, $\tau_c^* = 0.064\theta^{0.44}$ ($R^2 = 0.25$), into equation (5) to predict how the particle friction angle needs to change as a function of slope to explain the observed field data. Note that there is no physical reason to expect a power law relationship between τ_c^* and θ [e.g., *Lamb et al., 2008*], but for these field data from steep channels, it appears to be the most appropriate approximation. Figure 4a shows a wide range in possible trends between particle friction angle and slope for different values of lift-to-drag ratio and momentum loss to form drag. For any constant pair of values of F_L/F_D and τ_f/τ_b , it is expected that the particle friction angle will increase by $\sim 30^\circ$ between bed angles of $\theta = 0.1^\circ$ and 10° . Note that because *Lamb et al.’s [2008]* model attempts to account for reduced effectiveness of water flow in mobilizing sediment at steep slopes, the expected variations in friction angle with bed slope are conservative. For example, should the *Wiberg and Smith’s [1987]* model be used instead, friction angles would need to vary with bed angle over a much wider range to reconcile the model and observations.

Step low-order channels also tend to have narrow widths relative to the size of bed sediment. Results from flume experiments indicate that channel narrowing relative to grain size (i.e., decreasing jamming ratio: B/D_{84}) results in increased threshold Shields stress, independent of changes in bed slope [*Zimmermann, 2010*] (Figure 3). The experiments revealed that interlocking grains formed stable ribs (“steps”) across sufficiently narrow channel widths ($B/D_{84} < \sim 8$). Steps still formed at larger jamming ratios, but they were found to be less resistant to motion. The formation of steps has two hypothesized effects on the transport of sediment: increasing the particle friction angle of grains within the step [e.g., *Zimmermann et al., 2010*] and, subsequently, increasing the momentum lost to morphologic form drag [*Yager et al., 2012*]. We used a trust-region nonlinear optimization to find the best fit between threshold Shields stress and jamming ratio [*Zimmermann et al., 2010*]: $\tau_c^* = 0.12 + 0.45(B/D_{84})^{-2.1}$ ($R^2 = 0.39$). Note that the critical Shields stress is expected to be asymptotic to a base value of $\tau_c^* = 0.12$ for wide channels, which is reasonable for the typical bed slope of the *Zimmermann et al.’s [2010]* experiments ($\theta = 4.5^\circ$) [*Prancevic et al., 2014*]. Inputting this best fit relationship into equation (5)

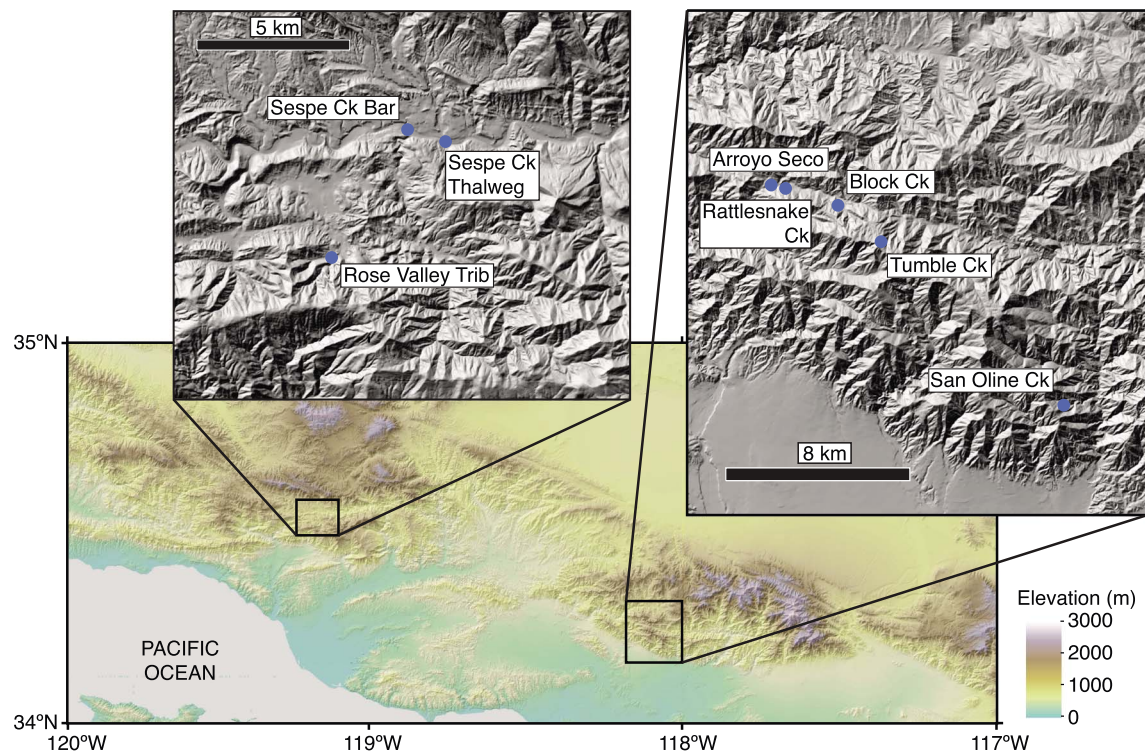


Figure 5. Location map of the study sites.

shows that particle friction angles are expected to decrease by $\sim 10^\circ$ with an increase in jamming ratio from $B/D_{84} = 2$ to 17 (Figure 4b). We did not extend these expectations outside of the tested range of Zimmermann *et al.* [2010]. Again, a wide range in curves results from the range of possible values of F_L/F_D and τ_F/τ_b .

3. Methods

3.1. Study Sites

We visited a total of eight field sites in Southern California during summer and fall of 2011 and 2013. The sites were located in either the San Gabriel Mountains (five sites total) or the Transverse Mountain Ranges (three sites total) in Southern California (Figure 5). The sites were chosen to test a wide variety of channel slopes ($\theta = 0.5^\circ$ to 23°), width-to-grain size ratios ($B/D_{84} = 9$ to 64), and fluvial sorting (Figure 6 and Table 2). Note that our smallest jamming ratio is larger than the critical jamming ratio proposed by Zimmermann *et al.* [2010], indicating that there should not be resistant force chains forming across the channel width. We timed visits to avoid any surface water, which would introduce ambiguity to measured pulling forces due to concomitant buoyancy and hydraulic forces. All sites but Sespe Thalweg and Sespe Bar exhibited signs of debris flow transport with incomplete fluvial sorting, consistent with their respective proximity to hillslopes and tributaries much steeper than the critical slope for en masse failure [Prancevic *et al.*, 2014]. At each site, we laid a measuring tape longitudinally along the thalweg of the channel extending 60 to 100 m. We measured the longitudinal profile of the sampling area along this tape using a laser range finder noting the presence of steps. Channel bed slope was calculated as the slope of the best fit line to each profile. At minimum, grain size distributions were calculated by sampling a grain at every meter along this measuring tape (i.e., grid-by-number [Bunte and Abt, 2001]). At some sites, an additional Woman pebble count of ~ 100 grains was performed (Data sets S2a to S2h in the supporting information). We also made measurements of channel width at each site. For Sespe Creek Bar and Sespe Creek Thalweg, the width was measured within a discernable elevated flooding surface (Figures 6a and 6b). Widths at Arroyo Seco, Block Creek, and Rattlesnake Creek were defined as the distance between debris flow levees (Figures 6d, 6e, and 6h). Rose Valley Tributary, San Oline Creek, and Tumble Creek were flanked on either side by steep hillslopes, and the channel width was defined by the zone of exposed coarse clasts between these hillslopes (Figures 6c, 6f, and 6g).

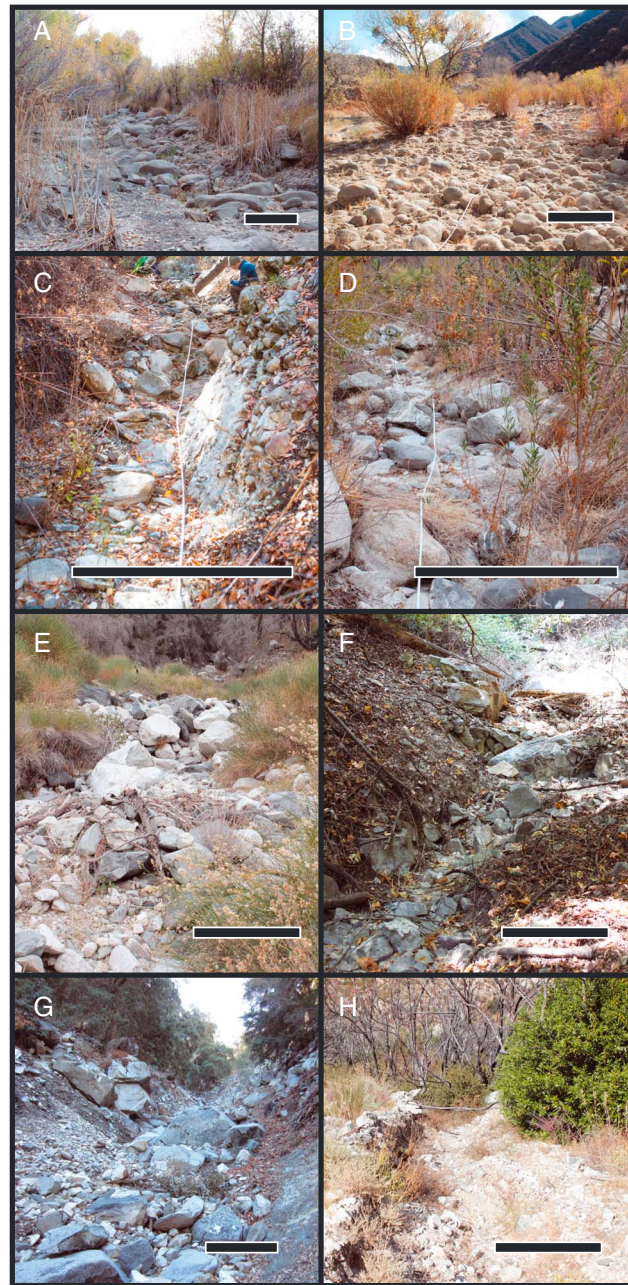


Figure 6. Representative photographs for all field sites. (a) Sespe Creek Thalweg, (b) Sespe Creek Bar, (c) Rose Valley Tributary, (d) Arroyo Seco, (e) Block Creek, (f) San Oline Creek, (g) Tumble Creek, and (h) Rattlesnake Creek. The scale bars correspond roughly to 1 m in the foreground.

distribution [Bunte and Abt, 2001]. Clasts were never skipped unless they were outside of our measurement force range, and a single clast was never measured twice.

In order to fasten the force gauge to the test grain, a length of webbing was wrapped around the grain and hooked to the force gauge. If the webbing could not be secured around the clast without disturbing interlocked neighboring grains, we drilled a 3/16" bolt into the clast and attached an eye bolt on which we could pull (Figure 9). Grains were pulled downstream, parallel to the inferred flow direction, and along an axis that passed approximately through the center of the exposed mass to mimic an evenly distributed fluid force. For each grain that was pulled, we also measured the three principal axes, the protrusion of the

Grain size distributions were broad at all sites (Figure 7), with large sorting coefficients ($\sigma \geq 0.9$) [Inman, 1952] (Table 2):

$$\sigma = \frac{1}{2} (\log_2 D_{84} - \log_2 D_{16}). \quad (6)$$

The median grain diameter for six of the eight sites is between 12 and 17 cm, while Sespe Creek Thalweg is considerably coarser ($D_{50} = 29$ cm), and Rattlesnake Creek is considerably finer ($D_{50} = 8$ cm). The channel widths generally narrow with increased slope, and consequently, steps occur preferentially in steeper reaches (Figure 8). One clear exception is Rattlesnake Creek, which sits close to the maximum slope for fluvial transport and shows no sorting into patches or steps (Figure 6h).

3.2. Boulder Pulling Methodology

In order to measure particle friction angles in situ, we utilized a handheld digital force gauge to measure the force required to dislodge a particle from its pocket and the weight of that particle (Figure 9). The force gauge is a Shimpo FGE-500HX, which has a 2500 N capacity (greater than our maximum pulling strength, which was limited to 2000 N under ideal pulling conditions), ± 5 N accuracy, and a sampling rate of 1000 Hz. The device records the peak force during the measurement period to prevent reading error while dislodging the clast. Early measurement attempts with a force gauge that did not record peak forces resulted in much smaller recorded pulling forces, indicating substantial error that may be present in other studies as well. Working upstream along the measuring tape used for the longitudinal profile, we sampled clasts over a regular 1 m spacing. This sampling scheme yields a grid-by-number friction angle

Table 2. Site Characteristics and Average Friction Angle

Site	Bed Angle, θ (deg)	Channel Width, B (m)	Grain Size, $D_{16}/D_{50}/D_{84}$ (cm)	Jamming Ratio, B/D_{84}	Sorting Coefficient, σ	Step Cover (%)	Friction Angle Measurements, n	Mean Normalized Friction Angle, $\bar{\phi}_N$ (deg)	Tenth Percentile Friction Angle, ϕ_{10} (deg)	Friction Angle Standard Deviation, s (deg)
Sespe Creek Thalweg	0.5	13	8.8/29/54	24	1.3	5	29	70.3	52.9	11.7
Sespe Creek Bar	0.7	16	6.0/14/25	64	1.0	0	31	70.0	48.0	14.5
Rose Valley Tributary	2.9	3	5.0/12/25	12	1.2	3	32	65.4	44.1	14.2
Arroyo Seco	3.7	4	7.0/16/29	14	1.0	30	35	71.4	58.5	12.8
Block Creek	8.4	5	4.4/15/29	17	1.4	8	33	70.7	51.5	13.2
San Oline Creek	9.1	2.5	9.0/17/29	9	0.9	16	33	65.6	49.6	13.7
Tumble Creek	17	6	5.5/16/41	15	1.5	25	36	65.4	47.6	14.5
Rattlesnake Creek	23	2	3.5/8.0/14	14	1.0	3	46	68.1	47.2	13.9

grain relative to the upstream channel bed, and the plain-view cross-sectional area exposed at the surface. We made qualitative notes of particle burial, imbrication, angularity, and wedging and recorded whether or not the particle was in a step, which we identified as width-spanning breaks in elevation dominantly composed of coarse ($>D_{50}$) clasts [Montgomery and Buffington, 1997].

During dislodgement, a dry particle experiences three forces: pulling force directed downstream (F_p), the downstream component of the weight vector ($W \sin \theta$), and the frictional resistance that is parameterized here using the bed-normal component of the weight ($\sum F_{n,i} = W \cos \theta$ in equation (1)). At the onset of motion, these forces balance along the downstream axis as

$$F_p + W \sin \theta = F_f = W \cos \theta \tan \phi. \tag{7}$$

Rearranging, the friction angle can be solved for explicitly as

$$\tan \phi = \tan \theta + \frac{F_p}{W \cos \theta}. \tag{8}$$

Because requisite pull force was typically higher than the weight, this led to a sampling bias at both ends of our data range. A boulder that weighs more than 2000 N will likely require a pull force higher than our strength limit and is effectively “stuck.” The largest grain successfully pulled at each site was between the 83rd and 100th percentiles of its respective grain size distribution. Conversely, a small pebble with a pull force of 10 N will likely have an irresolvable weight. The lower end bias was circumvented by using grain size measurements to estimate the weight, but estimating pull forces for the higher end bias is not possible, leading to a bias toward lower friction angles for coarse grains, on average.

4. Results

We collected a total of 275 data points within our range of measurable forces (Figure 10 and Data set S1 in the supporting information). The mobilization forces and particle weights vary over three orders of magnitude, reflecting the wide grain size distributions at each of these sites. The calculated friction angles vary between a modest $\phi = 27^\circ$ and a near-vertical $\phi = 89^\circ$, with sample standard deviations at each site ranging between $s = 12^\circ$ and 15° (Table 2). Note that equation (8) requires the force-to-weight ratio to be infinite to achieve a particle friction angle of $\phi = 90^\circ$. After normalizing the collected data to remove the observed relationship between ϕ and D/D_{50} , we

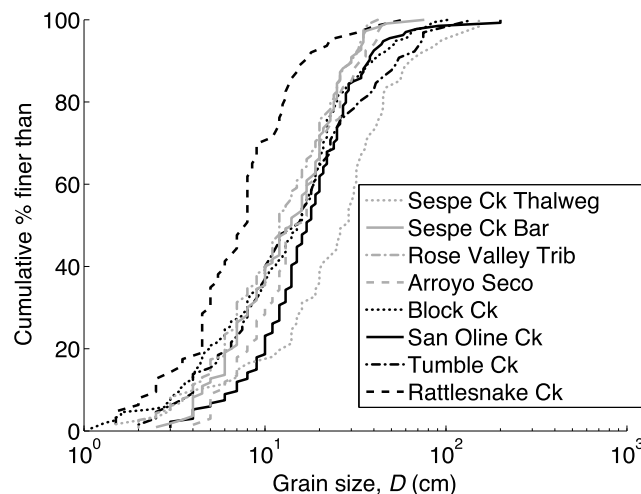


Figure 7. Grain size distributions for all sites.

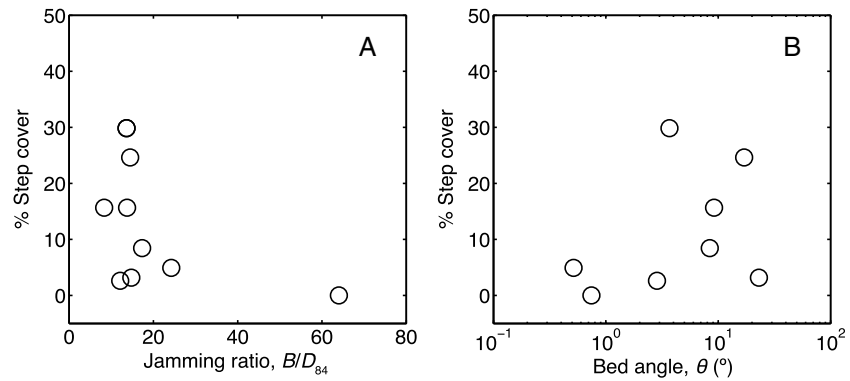


Figure 8. Percentage of the sampling grid composed of boulder steps for each site presented as a function of (a) jamming ratio and (b) channel slope.

tested for any additional dependence on other grain characteristics, slope, and jamming ratio in order to tease out the competing effects.

4.1. Particle Friction Angle and Grain Characteristics

To investigate the effect of relative grain size on particle friction angle at our study sites, in this section, we binned the data into four size classes with breaks at $D/D_{50} = 0.67, 1.0, \text{ and } 1.5$. Because our data points are distributed over several slopes and field sites, we grouped sites that exhibited similar trends between relative grain size and particle friction angle. A clear distinction in data existed between moderately sloping sites ($\theta < 5^\circ$) and steep sites ($\theta > 5^\circ$), and so we chose to group the data based on this criterion. To compare relative grain size effects across several sites, we divided all data by the mean particle friction angle of the median grain size at each site ($\phi/\phi_{D_{50}}$). This process helps to reduce some of the variability induced

by grouping sites together; however, variability due to small differences in trends (i.e., β) persists, and the global trend that results likely deviates slightly from the actual trend at each site.

The power law relationship between relative friction angle ($\phi/\phi_{D_{50}}$) and relative grain size (D/D_{50} , equation (2)) for these two slope regimes was calculated by performing a least squares linear regression on all data in log-log space. Binned geometric means are shown in linear space in Figure 11 for ease of viewing. Unlike most studies of particle friction angle [Miller and Byrne, 1966; Kirchner et al., 1990; Buffington et al., 1992; Johnston et al., 1998], our measured particle friction angles for $\theta < 5^\circ$ exhibits no trend with relative grain size outside of the standard error of $\beta = -0.014 \pm 0.032$ (Figure 11a and Table 1). This indicates that the trend between relative grain size and particle friction angle is muted compared to previous studies. A similarly muted trend was observed at the Pilgrim Creek and Colorado River sites in the study by Johnston et al. [1998] and is attributed to particle embedment. Data

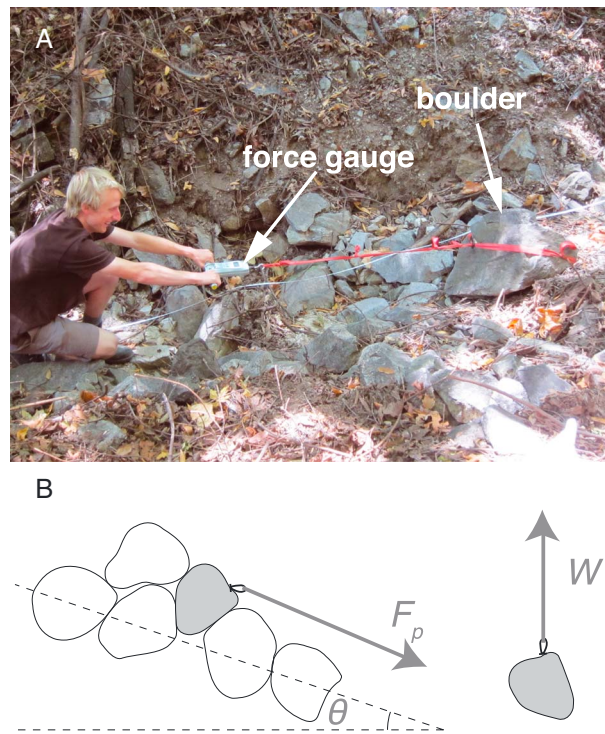


Figure 9. (a) Annotated photograph at San Oline Creek and (b) schematic of our setup for measuring the forces required to dislodge clasts (F_p), as well as weight (W).

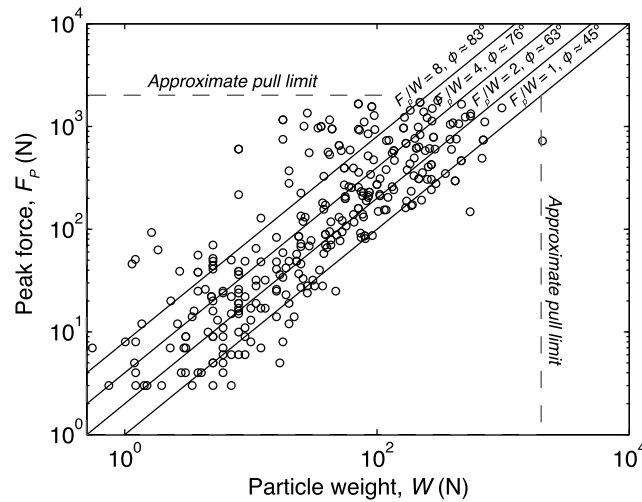


Figure 10. Peak force required for mobilization plotted against particle weight for all sites and measured clasts. The parallel solid lines indicate friction angle values assuming a horizontal bed. Actual values used in subsequent plots and analyses are slightly higher, reflecting the sloping bed (equation (7)). The dashed lines indicate the maximum force we were able to apply.

collected for $\theta > 5^\circ$ exhibit a trend closer to those previously published (Figure 11b), with $\beta = 0.180 \pm 0.032$. Still β is smaller in these channels than most previously reported values, both from tilt table experiments and Johnston et al.'s study of in situ particle friction angles (Table 1).

The tendency for larger-than-median grains to have lower particle friction angles is thought to be, in part, the result of larger grains resting on smaller grains with lower contact angles [Fenton and Abbott, 1977; Kirchner et al., 1990]. Within a natural streambed that lacks regular organization, relative grain size may not consistently predict the protrusion of a test grain from the bed. Grain protrusion, p , was measured independently in our field investigation as the maximum distance that the test grain extends above the bed surface (Data set S1 in the

supporting information), measured relative to the height of the bed one grain-length upstream of the high point of the test grain. The correlation between p/D and ϕ for our entire data set is poor ($R^2 = 0.05$), indicating that protrusion is not a good predictor of particle friction angle.

The Corey shape factor, $CSF = c/\sqrt{ba}$, where a , b , and c are the lengths of the maximum, intermediate, and minimum principal axes of the test grain, respectively, has also been shown to correlate with particle friction angle previously [Johnston et al., 1998]. However, the correlation between CSF and ϕ for our data set is also extremely poor ($R^2 = 0.006$).

In order to remove the relative grain size effect from the subsequent analyses, we define a normalized friction angle of each individual measurement: $\phi_N = \phi \left(\frac{D}{D_{50}}\right)^{-\beta}$, where $\beta = 0.180$ for $S > 5^\circ$ and $\beta = -0.014$ for $\theta < 5^\circ$. This normalization allows us to collapse all measurements to the expected friction angle for the median particle size and therefore allows us to test for the effects of channel slope and jamming ratio without covarying effects from D/D_{50} .

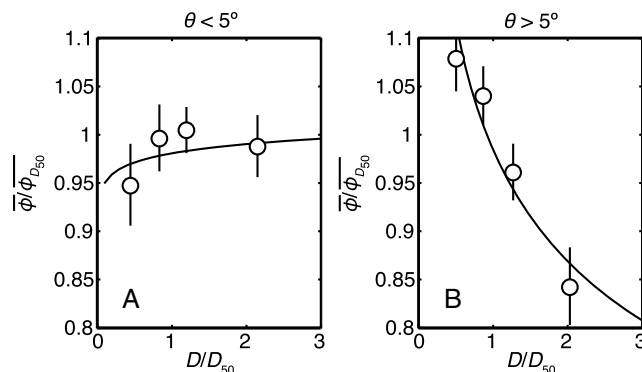


Figure 11. Mean particle friction angle as a function of relative grain size for (a) the relatively shallow sloping ($\theta < 5^\circ$) and (b) steep sites ($\theta > 5^\circ$). Friction angle values are normalized by the mean friction angle for the median grain size for each site. The error bars are the standard error of the measured values.

4.2. Particle Friction Angle and Channel Bed Slope

We compare the normalized friction angles averaged at each site ($\overline{\phi_N}$) against reach bed angle (θ) to test for slope dependence in particle friction angle at our sites. It should be noted that several studies have come to the logical conclusion that those grains with the lowest particle friction angle are the first to move and therefore the most important for describing incipient motion [Kirchner et al., 1990; Johnston et al., 1998; Schmeckle and Nelson, 2003]. The tenth percentile of each site's friction angle distribution, ϕ_{10} , generally scales with the mean (Table 2) and would yield

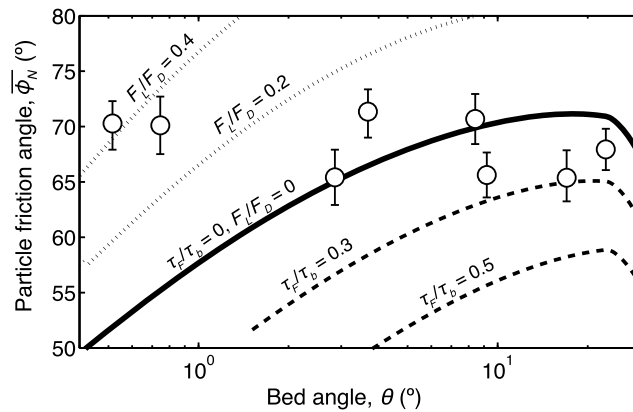


Figure 12. Mean normalized friction angle as a function of channel slope. The solid line is the model prediction (equation (4)) for no morphologic form drag and no lift force, as inverted from available field data. The dashed lines are the contours with no lift force but increasing morphologic form drag. The dotted lines are the contours with no form drag but increasing lift force.

similar findings in the subsequent analyses. However, due to the small number of data for each site, we use the mean normalized friction angle as a more robust characterization of the friction angle distribution.

Plotting the mean normalized friction angle and standard error versus bed slope reveals that grains are not more stable on steeper slopes for the sites visited in this study and that friction angle measurements do not match any of the predicted trends with constant values of F_L/F_D and τ_f/τ_b (Figure 12). No trend, positive or negative, exists outside of the standard error of our study sites, and the standard deviation observed at any given site is much higher than the range of average values when comparing between

sites (Table 2). The mean friction angles at all slopes are considerably higher than those previously reported for low-sloping channels and for tilt table measurements (Table 1).

4.3. Particle Friction Angle and Relative Width

In addition to channel bed slope, we compared the mean normalized friction angle, $\bar{\phi}_N$, to the jamming ratio, B/D_{84} , at each site. Step coverage within the channel increases sharply with decreased jamming ratio (Figure 8a). Also, the mean of the normalized particle friction angles of grains lodged in steps is statistically higher than that of grains measured outside of steps (two-sample t test, $p = 0.013$). In particular, histograms of normalized particle friction angles for grains in steps versus not in steps show that steps lack a small particle friction angle tail that is present in the rest of the data (Figure 13). Still, the mean particle friction angle does not appear to increase systematically with decreased jamming ratio (Figure 14). This is because steps only occupy a small portion of the channel bed and the grains in the tread between these steps tend to have low particle friction angles, balancing the average. For example, the mean normalized friction angle of grains outside of steps at San Oline Creek (63.2°) and Tumble Creek (63.0°), two sites with high step cover, were lower than any of the mean friction angles measured across the entire sites. Arroyo Seco was exceptional in that normalized friction angles were high both in steps (78.9°) and outside of steps (70.1°), although the mean in steps was higher.

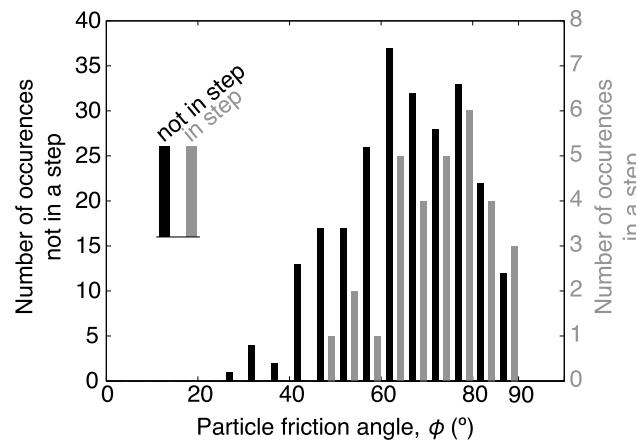


Figure 13. The number of particle friction angle measurements at all sites binned into 5° intervals for grains measured in steps (gray) and grains measured outside of steps (black).

5. Discussion

5.1. Particle Friction Angle and Bed Organization

One possible explanation for the muted trends between $\bar{\phi}/\bar{\phi}_{D_{50}}$ and D/D_{50} observed in Figure 11 is that the reach-scale D_{50} is a poor predictor of the grain sizes immediately surrounding a sampled clast. This is certainly true in fluvially sorted beds where patches quickly develop [e.g., Nelson et al., 2010; Scheingross et al., 2013]. Within an individual patch, a particular grain is more likely to be surrounded by grains of similar size rather than the reach D_{50} [Crowder and Diplas, 1997]. This should promote particle friction angles that are independent of grain size even when

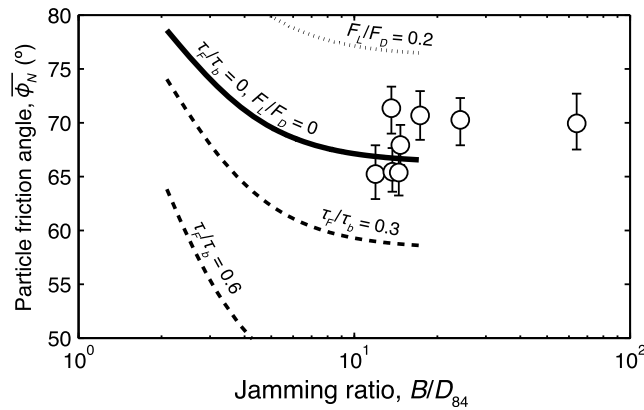


Figure 14. Mean friction angle as a function of jamming ratio. The solid line is the model prediction (equation (4)) for no morphologic form drag and no lift force, as inverted from available field data. The dashed lines are the contours with no lift force but increasing morphologic form drag. The dotted lines are the contours with no form drag but increasing lift force.

normalized by the reach D_{50} . While it is obvious that the D_{50} of the patch is the most appropriate length scale for comparison, characterizing grain size distributions over patches that are meter scale, as is common in low-order channels, is often not practicable for inferring reach-scale sediment transport rates.

The larger relative grain size dependence observed on steeper slopes (Figure 11b) is likely due to the reduced fluvial reorganization of the sediment beds in these reaches, which all show stronger evidence for debris flow deposition of grains, and lack sorting (Figure 6). Without substantial grain sorting, the reach D_{50} becomes more meaningful in describing the grains surrounding a sampled grain. For comparison, the previous study of in situ particle friction angles [Johnston et al., 1998] explicitly avoided portions of the channel bed that exhibited sorting or imbrication. Thus, the larger relative grain size dependence found at most sites of that study is consistent with our interpretation.

5.2. Size-Selective Transport

The effects of meter-scale bed organization also offer an explanation for the poor correlation between the reach sorting parameter (equation (6)) and the mean particle friction angle (Table 2), contrary to previous work [Buffington et al., 1992; Johnston et al., 1998]. It is likely that sorting at this smaller scale is partially responsible for the small differences in the mean particle friction angle between sites (Figures 12 and 14), and the reach sorting parameter does not capture these effects.

Large sediment grains should require higher bed shear stresses for mobilization than smaller ones if weight alone was important. Several studies have shown, however, that this size selectivity is diminished due to reduced particle friction angles and increased protrusion into the flow for larger grains [Mao et al., 2008; Parker, 2008; Yager et al., 2012; Scheingross et al., 2013]. This observation has led to the use of a “hiding function” to describe the degree of size selectivity in sediment transport [Parker, 1990]:

$$\frac{\tau_{bc}}{\tau_{bcD_{50}}} = \left(\frac{D}{D_{50}}\right)^{1-\gamma}, \tag{9}$$

where $\tau_{bcD_{50}}$ is the threshold bed shear stress to entrain the median grain size and γ is a nondimensional constant to describe how the threshold bed shear stress changes as a function of grain size. Note that $\gamma = 0$ indicates a linear correlation between sediment size and the threshold bed shear stress for entrainment and $\gamma = 1$ indicates that all grain sizes are mobile at the same bed shear stress (“size independence”). In a compilation of data from low-sloping channels, Parker [2008] suggests that channels are closer to size-independent transport, $\gamma = 0.79 \pm 0.16$ (standard deviation). Investigations in steep channels tend to report more size-selective values ranging from $\gamma = 0.51$ to 0.79 [Mao et al., 2008; Yager et al., 2012; Scheingross et al., 2013].

We can compare our grain size dependence on particle friction angle to these hiding functions by using the model of Lamb et al. [2008] and inputting measured slope, grain sizes, and friction angles for each channel.

For simplicity, the friction angle for each D/D_{50} at each site is calculated as $\bar{\phi} = \bar{\phi}_{D_{50}} \left(\frac{D}{D_{50}}\right)^{-\beta}$. The modeling suggests highly selective entrainment for the moderately sloping channels, $\gamma = 0.41$, and more peculiar behavior for the steepest channels (Figure 15). Within the steep channels examined here, the hiding effect is predicted to dominate for fine grains ($<D_{50}$), yielding reverse mobility, while coarse grains are predicted to exhibit highly size-selective transport. Some of the predicted size selectivity is the result of a strong dependence of the model on grain emergence from the flow surface in very steep channels [Lamb et al., 2008]. However, the muted grain size dependence in the particle friction angle appears to play an important role

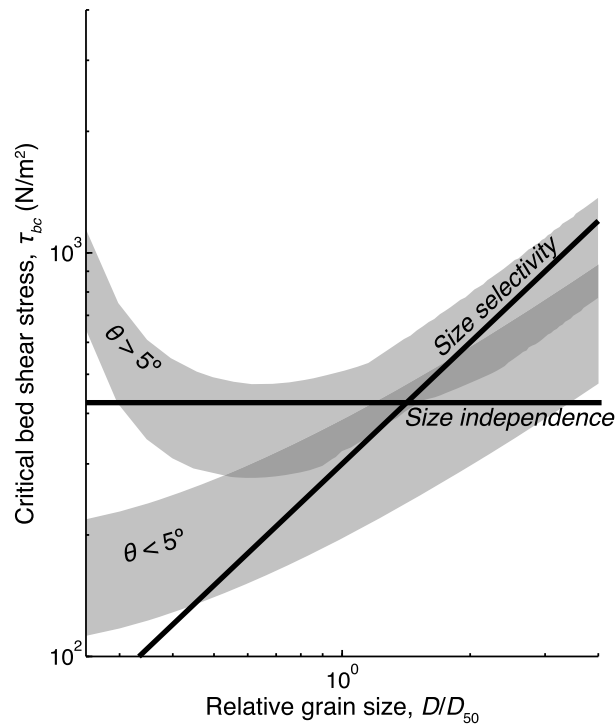


Figure 15. Model predictions for the critical basal shear stress required for a range of grain sizes at each site. The shaded regions indicate the distinct prediction envelopes for study sites with $\theta > 5^\circ$ and $\theta < 5^\circ$. The curves at each site were computed using equation (3); computed friction angle distributions (equation (2)); measured values of mean friction angle, channel slope, and grain size; and assumed values of $F_L/F_D = 0$ and $\tau_f/\tau_b = 0$.

trends between threshold Shields stress and bed slope [e.g., *Mueller et al., 2005; Mao et al., 2008*]. The consistency of mean particle friction angles over the wide range in bed slopes tested here suggests that changes in grain stability, on average, are not driving the observed trend of threshold Shields stress in the field. Instead, this trend is likely caused by changes in hydraulics inherent to shallow flows [e.g., *Lamb et al., 2008; Recking, 2009*], with a secondary effect due to changes in stress lost to morphologic form drag [e.g., *Wiberg and Smith, 1991; Millar, 1999; Nitsche et al., 2011; Ferguson, 2012; Yager et al., 2012; Scheingross et al., 2013*]. Because our data do not fall on any of the model contours in Figure 12, a change in morphologic form drag or lift-to-drag ratio is required to recover the observed trend in threshold Shields stresses in the field data.

5.4. Sediment Mobility and Jamming Ratio

Comparing mean particle friction angles with B/D_{84} similarly shows no trend (Figure 14). This result is consistent with the flume experiments of *Zimmermann et al. [2010]*, which did not produce considerable jamming above $B/D_{84} > \sim 8$. Still we observed greater step occurrence in narrower channels (Figure 8), and grains in these steps required twice the average normalized pulling strength ($\overline{F_p/W}$) to remove. Rather than stabilizing the entire channel bed, increased jamming ratio in our study sites promotes the stabilization of discrete steps. Once stabilized, these steps dramatically alter the hydraulics of the flow, increasing stress over the lip and into the plunge pool of the step and reducing stress over much of the lower-sloping step tread [*Zimmermann and Church, 2001*]. Thus, we suggest that particle friction angles inhibit sediment transport in narrow channels by increasing stability locally while focusing stress in the vicinity of the stable step.

5.5. Lift to Drag Ratios and Morphologic Form Drag

If the model predictions of particle friction angles based on observed threshold Shields stresses are correct, then this implies that lift-to-drag ratios and/or morphologic form drag must vary to reconcile the data sets (Figures 12 and 14). There are infinite combinations of F_L/F_D and τ_f/τ_b that could potentially explain the

in size selectivity, particularly at the moderately steep slopes. These results help to reconcile the abundant observations of size-selective transport in mountain channels [e.g., *Lenzi et al., 1999, 2006b; Mao et al., 2008; Scheingross et al., 2013*] with the theory that predicts that large grains should be as mobile as or even more mobile than small grains [e.g., *Egiazaroff, 1965; Wiberg and Smith, 1987; Solari and Parker, 2000; Parker, 2008*]. This increase in size selectivity ultimately renders the largest grains immobile and promotes extraction of momentum from the flow, increasing the bed shear stress required for mobilization and reducing sediment transport rates [*Yager et al., 2007*].

5.3. Sediment Mobility and Channel Bed Slope

Over the eight sites we studied, with bed angles ranging from $\theta = 0.5^\circ$ to 23° , there was no trend between particle friction angle and bed slope (Figure 12). To reject the hypothesis that the increased threshold Shields stress with increased slope is due to increased particle friction angles, corresponding measurements of the threshold Shields stress at our study sites would be ideal. In the absence of such data, however, we rely on previously established

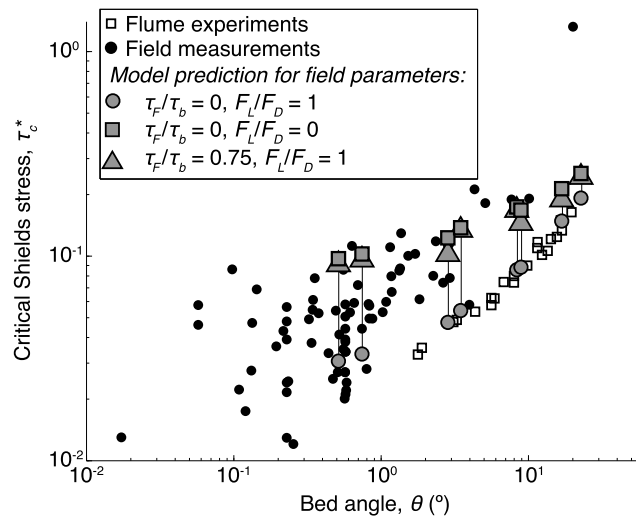


Figure 16. Computed critical Shields stress for the measured friction angles and respective slopes using equation (3) and various values of F_L/F_D and τ_f/τ_b . Field [Andrews, 1994; Buffington and Montgomery, 1997; Andrews, 2000; Church and Hassan, 2002; Whitaker and Potts, 2007; Mao et al., 2008; Scheingross et al., 2013] and flume [Prancevic et al., 2014] data from Figure 2 are included for comparison.

streams of varying slope and width, we were able to assess the effect of these parameters on the particle friction angle. Interestingly, median grain sizes over all slopes in this study are, on average, more stable than previously recorded. This is likely due to the effects of particle interlocking that are necessarily ignored in tilt table measurements. In addition, friction angle measurements made in situ do not exhibit as pronounced a grain size dependence as those derived from tilt table experiments. This indicates that coarse grains are less easily mobilized than previously thought within our study sites. Increased grain stability was also observed in steps. Even so, the particle friction angle did not vary systematically with either slope or jamming ratio (above the critical value proposed by Zimmermann et al. [2010]), indicating that the threshold bed shear stress required to mobilize sediment at our study sites would not increase as a direct result of particle friction angles. Instead, an increase in threshold bed shear stress should result from changing hydraulics in steep channels, including an increase in momentum loss to immobile boulders and bed forms. It is also likely that the offset between the threshold bed shear stress for sediment mobilization in the laboratory versus the field is due to the heightened particle friction angles in natural channels, although firm conclusions are hindered by a lack of theory for lift forces and morphologic form drag in shallow and steep flows. This work illustrates the importance of the heterogeneity of particle friction angles in natural channels, which can only be observed if measured in situ.

Notation

- B channel width
- C_D drag coefficient
- D length of intermediate grain axis
- D_n n th percentile grain diameter
- F_D drag force
- F_L lift force
- F_N normal force
- F_P pulling force
- F_R frictional force
- g gravitational acceleration
- H flow depth
- u local time-averaged velocity

available field data. Figure 16 shows that by varying either parameter while holding the other constant, we can recover nearly the entire envelope of threshold Shields stresses observed in the field. In reality, both parameters are likely changing. The experiments of Schmeckle et al. [2007] reveal considerable scatter in the lift force and do not support a generalized ratio between lift and drag force. In addition, our own results support slope-dependent morphologic form drag through stabilization of coarse grains and steps preferentially on steep slopes. More work is needed to constrain the role of these two parameters in reducing sediment transport rates.

6. Conclusions

By directly measuring the force required to dislodge 275 sediment grains in eight

u^*	shear velocity
V	grain volume
W	grain weight
z	bed-normal spatial coordinate
β	friction angle fit parameter
γ	critical shear stress fit parameter
δ	geometrical grain exposure factor
θ	bed angle
ρ	density of water
ρ_s	material density of sediment
σ	grain sorting parameter
σ_u	temporal standard deviation of flow velocity
τ_b	total bed shear stress
τ_{bc}	total bed shear stress at the onset of motion
$\tau_{bcD_{50}}$	total bed shear stress at the onset of motion of the median grain size
τ^*	Shields stress
τ_c^*	Shields stress at the onset of motion
τ_F	bed shear stress expended on immobile obstacles
ϕ	particle friction angle
$\phi_{D_{50}}$	friction angle of the median grain size ($2/3D_{50} \leq D < 3/2D_{50}$)
ϕ_N	grain-size-normalized particle friction angle

Acknowledgments

Preliminary measurements for this study were performed by Eric Kleinsasser. We would like to thank Brian Fuller, Luca Malatesta, Joel Scheingross, and Alison Piasecki for their help with field measurements. Field data and calculated friction angles can be found in the supporting information. Funding for this work was provided by NSF grants EAR-0922199 and EAR-1349115, the Terrestrial Hazards Observation and Reporting center at Caltech, and the Keck Institute for Space Studies. We thank Michael Church, Mark Schmeckle, and an anonymous reviewer for their insightful reviews that improved this paper.

References

- Aberle, J., and G. M. Smart (2003), The influence of roughness structure on flow resistance on steep slopes, *J. Hydraul. Res.*, *41*(3), 259–269, doi:10.1080/00221680309499971.
- Andrews, E. D. (1994), Marginal bed load transport in a gravel bed stream, Sagehen Creek, California, *Water Resour. Res.*, *30*(7), 2241–2250, doi:10.1029/94WR00553.
- Andrews, E. D. (2000), Bed material transport in the Virgin River, Utah, *Water Resour. Res.*, *36*(2), 585–596, doi:10.1029/1999WR900257.
- Ashida, K., and M. Bayazit (1973), Initiation of motion and roughness of flows in steep channels, *Hydraul. Proc. 15th Congress. Istanbul, Turkey*, *1*, 475–484.
- Bartnick, W. (1991), Determination of the critical conditions of incipient motion of bed load in mountain rivers, in *Fluvial Hydraulics in Mountain Regions*, edited by A. Armanini and G. Di Silvio, pp. 83–88, Springer, Berlin.
- Bathurst, J. C., H. H. Cao, and W. H. Graf (1984), Hydraulics and sediment transport in a steep flume: Data from the EPFL study, Report, Centre for Ecology and Hydrology, Wallingford, U. K.
- Brummer, C., and D. Montgomery (2003), Downstream coarsening in headwater channels, *Water Resour. Res.*, *39*(10), 1294, doi:10.1029/2003WR001981.
- Buffington, J. M., W. E. Dietrich, and J. W. Kirchner (1992), Friction angle measurements on a naturally formed gravel streambed: Implications for critical boundary shear stress, *Water Resour. Res.*, *28*(2), 411–425, doi:10.1029/91WR02529.
- Bunte, K., and S. R. Abt (2001), Sampling surface and subsurface particle-size distributions in wadable gravel- and cobble-bed streams for analyses in sediment transport, hydraulics, and streambed monitoring, USDA Forest Service.
- Carollo, F., V. Ferro, and D. Termini (2005), Analyzing turbulence intensity in gravel bed channels, *J. Hydraul. Eng.*, *131*(12), 1050–1061, doi:10.1061/(ASCE)0733-9429(2005)131:12(1050).
- Church, M., and M. A. Hassan (2002), Mobility of bed material in Harris Creek, *Water Resour. Res.*, *38*(11), 1237, doi:10.1029/2001WR000753.
- Church, M., M. A. Hassan, and J. F. Wolcott (1998), Stabilizing self-organized structures in gravel-bed stream channels: Field and experimental observations, *Water Resour. Res.*, *34*(11), 3169–3179, doi:10.1029/98WR00484.
- Coulombe-Pontbriand, M., and M. Lapointe (2004), Landscape controls on boulder-rich, winter habitat availability and their effects on Atlantic salmon (*Salmo salar*) parr abundance in two fifth-order mountain streams, *Can. J. Fish. Aquat. Sci.*, *61*(4), 648–658, doi:10.1139/F04-023.
- Crowder, D. W., and P. Diplas (1997), Sampling heterogeneous deposits in gravel-bed streams, *J. Hydraul. Eng.*, *123*(12), 1106–1117, doi:10.1061/(ASCE)0733-9429(1997)123:12(1106).
- D'Agostino, V., and M. A. Lenzi (1999), Bedload transport in the instrumented catchment of the Rio Cordon, *Catena*, *36*(3), 191–204, doi:10.1016/S0341-8162(99)00017-X.
- Downes, B. J., A. Glaister, and P. S. Lake (1997), Spatial variation in the force required to initiate rock movement in 4 upland streams: Implications for estimating disturbance frequencies, *J. N. Am. Benthol. Soc.*, *16*, 203–220, doi:10.2307/1468252.
- Egiazaroff, I. V. (1965), Calculation of nonuniform sediment concentrations, *J. Hydraul. Div. Am. Soc. Civ. Eng.*, *91*(4), 225–247.
- Fenton, J. D., and J. E. Abbott (1977), Initial movement of grains on a stream bed: The effect of relative protrusion, *Proc. R. Soc. London A. Math. Phys. Sci.*, *352*(1671), 523–537.
- Ferguson, R. I. (2012), River channel slope, flow resistance, and gravel entrainment thresholds, *Water Resour. Res.*, *48*, W05517, doi:10.1029/2011WR010850.
- Gilbert, G. K. (1914), The transportation of debris by running water, *U.S. Geol. Surv. Prof. Pap.*, *86*, 263.
- Graf, W. H., and L. Suszka (1987), Sediment transport in steep channels, *J. HydroSci. Hydraul. Eng.*, *5*(1), 11–26.
- Gregoretti, C. (2008), Inception sediment transport relationships at high slopes, *J. Hydraul. Eng.*, *134*(11), 1620–1629, doi:10.1061/(ASCE)0733-9429(2008)134:11(1620).
- Inman, D. L. (1952), Measures for describing the size distribution of sediments, *J. Sediment. Res.*, *22*(3), 125–145.

- Johnston, C. E., E. D. Andrews, and J. Pitlick (1998), In situ determination of particle friction angles of fluvial gravels, *Water Resour. Res.*, *34*(8), 2017–2030, doi:10.1029/98WR00312.
- Kirchner, J. W., W. E. Dietrich, F. Iseya, and H. Ikeda (1990), The variability of critical shear stress, friction angle, and grain protrusion in water-worked sediments, *Sedimentology*, *37*, 647–672, doi:10.1111/j.1365-3091.1990.tb00627.x.
- Kostaschuk, R., P. Villard, and J. Best (2004), Measuring velocity and shear stress over dunes with acoustic Doppler profiler, *J. Hydraul. Eng.*, *130*(9), 932–936, doi:10.1061/(ASCE)0733-9429(2004)130:9(932).
- Lamb, M. P., W. E. Dietrich, and J. G. Venditti (2008), Is the critical Shields stress for incipient sediment motion dependent on channel-bed slope? *J. Geophys. Res.*, *113*, F02008, doi:10.1029/2007JF000831.
- Laronne, J. B. (1973), *A Geomorphological Approach to Coarse Bed Material Movement in Alluvial Channels, With Special Reference to a Small Appalachian Stream*, pp. 1–219, McGill Univ., Montreal, QC, 6 August.
- Lenzi, M. A., V. D'Agostino, and P. Billi (1999), Bedload transport in the instrumented catchment of the Rio Cordon, *Catena*, *36*(3), 171–190, doi:10.1016/S0341-8162(99)00016-8.
- Lenzi, M. A., L. Mao, and F. Comiti (2006a), Effective discharge for sediment transport in a mountain river: Computational approaches and geomorphic effectiveness, *J. Hydrol.*, *326*(1–4), 257–276, doi:10.1016/j.jhydrol.2005.10.031.
- Lenzi, M. A., L. Mao, and F. Comiti (2006b), When does bedload transport begin in steep boulder-bed streams?, *Hydrol. Processes*, *20*, 3517–3533, doi:10.1002/hyp.6168.
- Li, Z., and P. D. Komar (1986), Laboratory measurements of pivoting angles for applications to selective entrainment of gravel in a current, *Sedimentology*, *33*(3), 413–423, doi:10.1111/j.1365-3091.1986.tb00545.x.
- Major, J. J. (1997), Depositional processes in large-scale debris-flow experiments, *J. Geol.*, *105*(3), 345–366.
- Mao, L., G. P. Uyttendaele, A. Iroumé, and M. A. Lenzi (2008), Field based analysis of sediment entrainment in two high gradient streams located in Alpine and Andine environments, *Geomorphology*, *93*(3), 368–383, doi:10.1016/j.geomorph.2007.03.008.
- Meyer-Peter, E., and R. Mueller (1948), Formulas for bed-load transport, *Proc. 2nd Congr. Int. Assoc. Hydraul. Res., Stockholm*, 39–64.
- Millar, R. G. (1999), Grain and form resistance in gravel-bed rivers, *J. Hydraul. Res.*, *37*(3), 303–312, doi:10.1080/00221686.1999.9628249.
- Miller, R. L., and R. J. Byrne (1966), The angle of repose for a single grain on a fixed rough bed, *Sedimentology*, *6*(4), 303–314, doi:10.1111/j.1365-3091.1966.tb01897.x.
- Montgomery, D., and J. Buffington (1997), Channel-reach morphology in mountain drainage basins, *Geol. Soc. Am. Bull.*, *109*(5), 596–611, doi:10.1130/0016-7606(1997)109<0596:CRMIMD>2.3.CO;2.
- Mueller, E. N., R. J. Batalla, C. Garcia, and A. Bronstert (2008), Modeling bed-load rates from fine grain-size patches during small floods in a gravel-bed river, *J. Hydraul. Eng.*, *134*(10), 1430–1439, doi:10.1061/(ASCE)0733-9429(2008)134:10(1430).
- Mueller, E. R., J. Pitlick, and J. M. Nelson (2005), Variation in the reference Shields stress for bed load transport in gravel-bed streams and rivers, *Water Resour. Res.*, *41*, W04006, doi:10.1029/2004WR003692.
- Nelson, P. A., W. E. Dietrich, and J. G. Venditti (2010), Bed topography and the development of forced bed surface patches, *J. Geophys. Res.*, *115*, F04024, doi:10.1029/2010JF001747.
- Nikora, V., D. Goring, I. McEwan, and G. Griffiths (2001), Spatially averaged open-channel flow over rough bed, *J. Hydraul. Eng.*, *127*(2), 123–133, doi:10.1061/(ASCE)0733-9429(2001)127:2(123).
- Nitsche, M., D. Rickenmann, J. M. Turowski, A. Badoux, and J. W. Kirchner (2011), Evaluation of bedload transport predictions using flow resistance equations to account for macro-roughness in steep mountain streams, *Water Resour. Res.*, *47*, W08513, doi:10.1029/2011WR010645.
- Olivero, M. (1984), Movimiento incipiente de partículas en flujo torrencial, *Special Report: University of Los Andes, Meridad, Venezuela*, 1–169.
- Parker, G. (1990), Surface-based bedload transport relation for gravel rivers, *J. Hydraul. Res.*, *28*(4), 417–436, doi:10.1080/00221689009499058.
- Parker, G. (2008), Transport of gravel and sediment mixtures, in *American Society of Civil Engineering Manual*, pp. 165–251, American Society of Civil Engineers, Reston, Va.
- Picon, G. A. (1991), Estudio experimental de transporte sedimentos en rios de montaña, Universidad de Los Andes, Merida, Venezuela, 2 July.
- Prancevic, J. P., M. P. Lamb, and B. M. Fuller (2014), Incipient sediment motion across the river to debris-flow transition, *Geology*, *42*, 191–194, doi:10.1130/G34927.1.
- Recking, A. (2009), Theoretical development on the effects of changing flow hydraulics on incipient bed load motion, *Water Resour. Res.*, *45*, W04401, doi:10.1029/2008WR006826.
- Rickenmann, D. (1997), Sediment transport in Swiss torrents, *Earth Surf. Processes Landforms*, *22*, 937–951, doi:10.1002/(SICI)1096-9837(199710)22:10<937::AID-ESP786>3.3.CO;2-I.
- Rickenmann, D. (2012), Alluvial steep channels: Flow resistance, bedload transport prediction, and transition to debris flows, in *Gravel-Bed Rivers*, pp. 386–397, John Wiley, Chichester, U. K.
- Sanguinito, S., and J. Johnson (2011), Quantifying gravel overlap and dislodgement forces on natural river bars: Implications for particle entrainment, *Earth Surf. Processes Landforms*, *37*(1), 134–141, doi:10.1002/esp.2237.
- Scheingross, J. S., E. W. Winchell, M. P. Lamb, and W. E. Dietrich (2013), Influence of bed patchiness, slope, grain hiding, and form drag on gravel mobilization in very steep streams, *J. Geophys. Res. Solid Earth*, *118*, 1–20, doi:10.1002/jgrf.20067.
- Schmeeckle, M. W., and J. M. Nelson (2003), Direct numerical simulation of bedload transport using a local, dynamic boundary condition, *Sedimentology*, *50*(2), 279–301.
- Schmeeckle, M. W., J. M. Nelson, and R. L. Shreve (2007), Forces on stationary particles in near-bed turbulent flows, *J. Geophys. Res.*, *112*, F02003, doi:10.1029/2006JF000536.
- Shields, A. (1936), Anwendung der Ähnlichkeitsmechanik und der turbulenzforschung auf die geschiebebewegung, *Mitt. Preuss Versuchsanst. Wasserbau Schiffbau*, *26*.
- Shvidchenko, A. B., and G. Pender (2000), Flume study of the effect of relative depth on the incipient motion of coarse uniform sediments, *Water Resour. Res.*, *36*(2), 619–628, doi:10.1029/1999WR900312.
- Sklar, L. S., and W. E. Dietrich (2004), A mechanistic model for river incision into bedrock by saltating bed load, *Water Resour. Res.*, *40*, W06301, doi:10.1029/2003WR002496.
- Smith, J. D., and S. R. Mclean (1977), Spatially averaged flow over a wavy surface, *J. Geophys. Res.*, *82*(12), 1735–1746, doi:10.1029/JC082i012p01735.
- Solari, L., and G. Parker (2000), The curious case of mobility reversal in sediment mixtures, *J. Hydraul. Eng.*, *126*(3), 185–197, doi:10.1061/(ASCE)0733-9429(2000)126:3(185).
- Stock, J. D., and W. E. Dietrich (2006), Erosion of steepland valleys by debris flows, *Geol. Soc. Am. Bull.*, *118*(9–10), 1125–1148, doi:10.1130/B25902.1.
- Torri, D., and J. Poesen (1988), Incipient motion conditions for single rock fragments in simulated rill flow, *Earth Surf. Processes Landforms*, *13*(3), 225–237, doi:10.1002/esp.3290130304.

- Whitaker, A. C., and D. F. Potts (2007), Analysis of flow competence in an alluvial gravel bed stream, Dupuyer Creek, Montana, *Water Resour. Res.*, *43*, W07433, doi:10.1029/2006WR005289.
- Wiberg, P. L., and J. D. Smith (1987), Calculations of the critical shear stress for motion of uniform and heterogeneous sediments, *Water Resour. Res.*, *23*(8), 1471–1480, doi:10.1029/WR023i008p01471.
- Wiberg, P. L., and J. D. Smith (1991), Velocity distribution and bed roughness in high-gradient streams, *Water Resour. Res.*, *27*(5), 825–838, doi:10.1029/90WR02770.
- Yager, E. M., J. W. Kirchner, and W. E. Dietrich (2007), Calculating bed load transport in steep boulder bed channels, *Water Resour. Res.*, *43*, W07418, doi:10.1029/2006WR005432.
- Yager, E. M., W. E. Dietrich, J. W. Kirchner, and B. W. McArdeil (2012), Prediction of sediment transport in step-pool channels, *Water Resour. Res.*, *48*, W01541, doi:10.1029/2011WR010829.
- Zimmermann, A. (2010), Flow resistance in steep streams: An experimental study, *Water Resour. Res.*, *46*, W09536, doi:10.1029/2009WR007913.
- Zimmermann, A., and M. Church (2001), Channel morphology, gradient profiles, and bed stresses during flood in a step-pool channel, *Geomorphology*, *40*, 311–327, doi:10.1016/S0169-555X(01)00057-5.
- Zimmermann, A., M. Church, and M. A. Hassan (2010), Step-pool stability: Testing the jammed state hypothesis, *J. Geophys. Res.*, *115*, F02008, doi:10.1029/2009JF001365.